Th. 1645

LA-6936-MS
Informal Report

UC-25 and UC-28
Issued: November 1977

Steady-State Temperature and Stress Distributions of a Proposed LAMPF Pyrolytic Graphite Pion Production Target

Lloyd O. Lindquist
Edward C. Scarbrough

los alamos
scientific laboratory
of the University of California
LOS ALAMOS, NEW MEXICO 87545

An Affirmative Action/Equal Opportunity Employer

UNITED STATES
DEPARTMENT OF ENERGY
CONTRACT W-7405-ENG. 36

STEADY-STATE TEMPERATURE AND STRESS DISTRIBUTIONS OF A PROPOSED LAMPF PYROLYTIC GRAPHITE PION PRODUCTION TARGET

by

Lloyd O. Lindquist and Edward C. Scarbrough

ABSTRACT

Two target configurations, suitable for the Clinton P. Anderson Meson Physics Facility (LAMPF) pion production sites, are analyzed for maximum temperatures and stresses to be experienced at LAMPF's design current (800-MeV protons at 1-mA average current).

A steady-state analysis is performed using the computer code TSAAS. The pulsed nature of the beam is not considered (6% duty). Both targets are pyrolytic graphite. One is cooled by water flowing through copper tubes bonded to the graphite; the other is cooled by water flowing through holes drilled in a copper layer bonded to the graphite.

Results of both analyses indicate that the calculated maximum stresses in the heated zone and at the copper/graphite interface due to proton beam heating are substantially lower than published values of the ultimate tensile and compressive strengths of pyrolytic graphite and copper. The calculated hot-spot temperatures are below the maximum temperature allowed by evaporation loss considerations.

I. INTRODUCTION

In 1979, the Clinton P. Anderson Meson Physics Facility (LAMPF) plans to begin operating the facility at design current (800-MeV protons at an average current of 1 mA). Calculations[1,2] show that the nonspinning, radiatively cooled graphite targets at the A-1 and A-2 pion production areas will reach a hot-spot temperature of 2300 K at an average beam current of about 0.5 mA. The targets will begin to evaporate at an unacceptable rate at this temperature (Fig. 1 gives the evaporation-rate curve for graphite). A study was initiated to develop new target configurations which will meet the requirements of the milliampere beam conditions.

This report presents the results of a steady-state thermal-stress analysis of a proposed target configuration suitable for the LAMPF A-1, A-2, or A-5 pion production area. The target (Fig. 2) is analyzed using the computer code TSAAS[3] for maximum temperatures and stresses to be experienced under maximum LAMPF beam current (1 mA). The target modeled is pyrolytic graphite with fixed-temperature boundary conditions simulating the effect of water cooling at

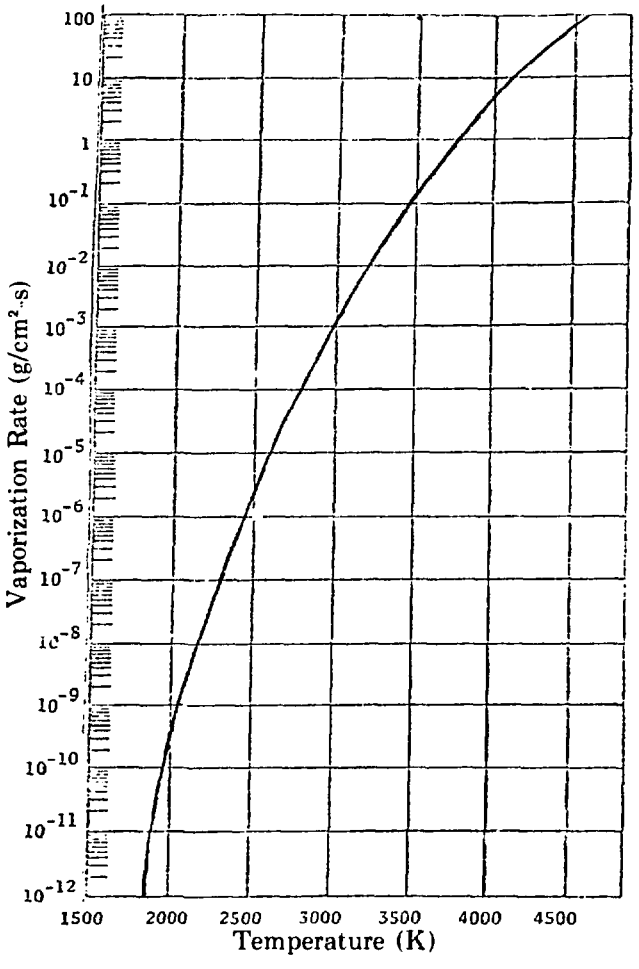

Fig. 1.
Graphite evaporation rate vs temperature of graphite surface.

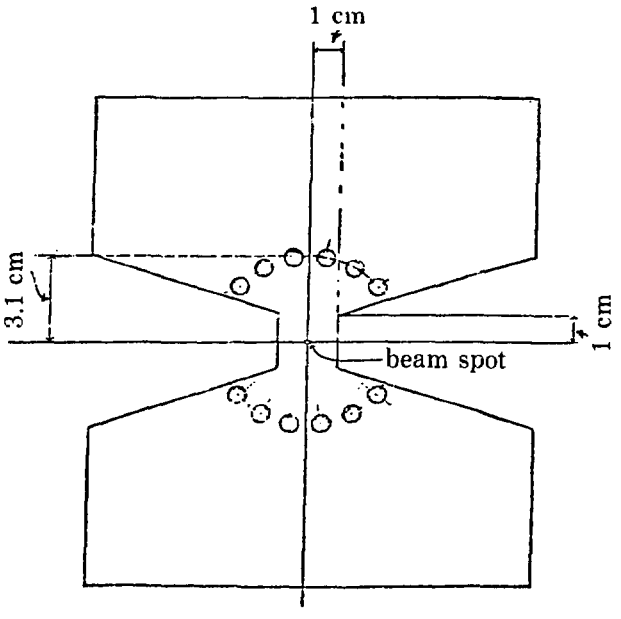

Fig. 2(a).
Front view of water-cooled pyrolytic graphite target.

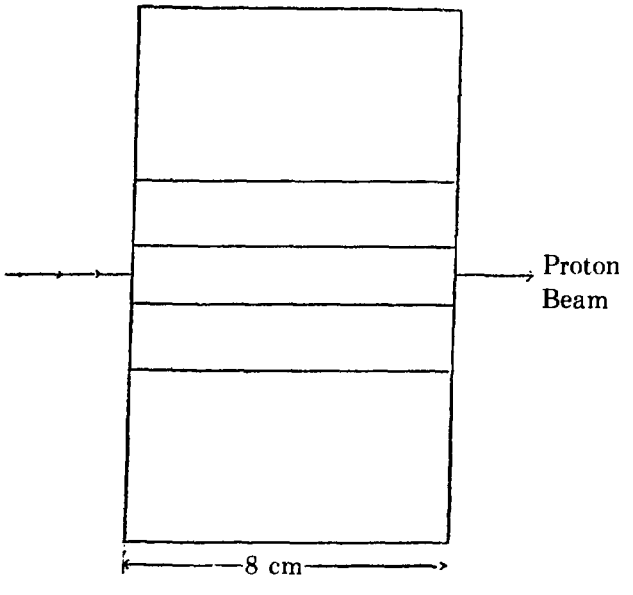

Fig. 2(b).
Side view of water-cooled pyrolytic graphite target.

the boundaries. An alternate design (Fig. 3), in which water-cooled copper is bonded to pyrolytic graphite, is also treated. The maximum temperatures and stresses calculated in both cases are presented in Table I. These results indicate that the pyrolytic graphite target should withstand a constant heat deposition of 40 kW, the power deposition of the 800-MeV protons in an 8-cm-thick pyrolytic graphite target at LAMPF's design current.

It should be noted that this analysis deals only with a constant heat flux. The pulsed nature of the beam is not considered. A transient analysis using TSAAS is being completed to determine the thermal-stress effects of the beam macropulse structure.

II. PYROLYTIC GRAPHITE

The first target configuration analyzed is shown in Fig. 2. It is composed of pyrolytic graphite, cooled by water flowing through copper tubes bonded to the graphite. The I-beam structure was chosen for several reasons.

- The shape allows the target to be inserted or removed without undesirable material (such as copper or water) interacting with the proton beam.
- The shape provides a minimum of interference with the experimental channels.
- There is no excess material between the place where pions are born in the proton target and the experimental channel that will use the pions.
- Multiple scattering and loss in energy are minimized.
- The circular arc of cooling tubes provides an isothermal heat transfer interface to eliminate heat flux gradients at the cooling interface.

The geometry of Fig. 2 is unnecessarily complicated for use in the TSAAS analysis. Figure 4 is an excellent thermal representation; it preserves the important features of Fig. 2 while having a relatively simple geometry. A quarter section of the target is analyzed, since the proton beam

TABLE I

MOST SIGNIFICANT RESULTS OF THERMAL STRESS ANALYSIS

Target	Maximum Temperature (K)	Maximum Stress (N/m^2)
Water-cooled graphite	696	[a]0.51×10^7
Water-cooled copper bonded to graphite - Graphite	757	[a]0.12×10^8
Copper	416	[a]0.51×10^8

Sublimation temperature of pyrolytic graphite	= 3925 K
Ultimate tensile strength of graphite	= 10^8 N/m^2
Ultimate compressional strength of graphite	= 10^6 N/m^2
Yield strength of Copper	$\simeq 3 \times 10^6$ N/m^2 (underestimate)

[a]In compression.

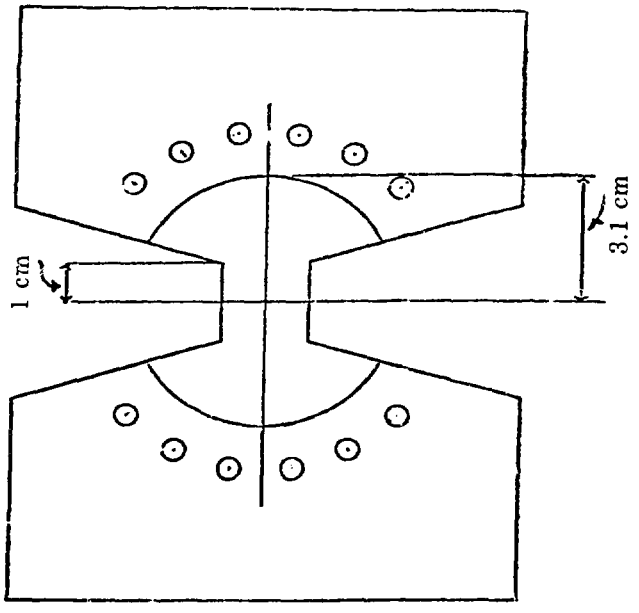

Fig. 3.
Water-cooled copper layer, bonded to graphite target.

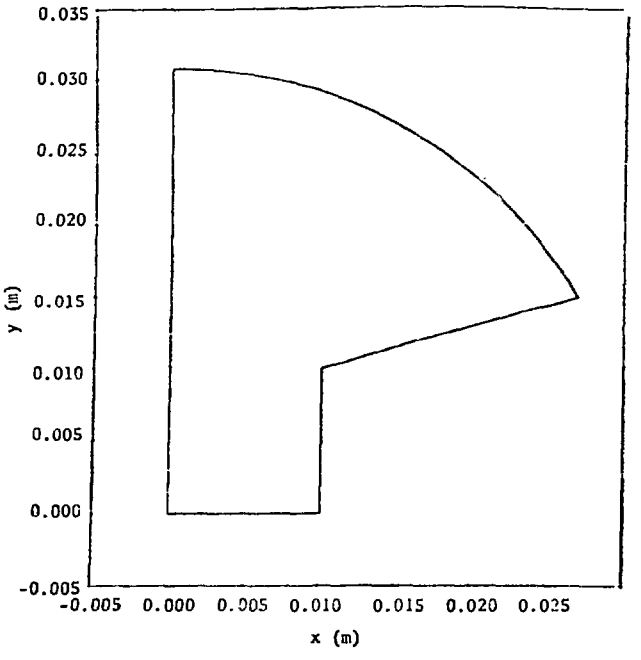

Fig. 4.
Target geometry, used in TSAAS analysis.

axis lies at the intersection of the lines of symmetry. There is no net heat transfer across the lines of symmetry.* The approximations made in using Fig. 4 are given below.

The structural, or "a-b," planes of the pyrolytic graphite are oriented perpendicular to the beam axis. This leads to a relatively short thermal path between the hot spot and the cooling interface.** Hence, the arc of tubes can be thermally approximated by a circular boundary of constant temperature, where one assumes that water flows across the entire boundary. In addition, the change in energy loss of the protons along the thickness of the target is about 1% (see Sec. III). Assuming uniform power deposition in the proton target, there will be no temperature gradient along the beam axis; the thermal stresses between planes should be minimal and are not calculated.

A planar analysis, neglecting the stresses in the direction of the beam, is the focus of this calculational study.†

III. BEAM HEATING

The total power dissipated in the proton target is 40 kW (10 kW over the quarter section that was analyzed). This number was derived in the following way:

*Unless otherwise stated, material boundaries bordering on unspecified media are considered perfect insulators.

**The thermal conductivity of pyrolytic graphite in the a-b plane is better than that of copper.

†In a planar analysis, the target is assumed to be of unit thickness.

The energy loss per unit distance of an 800-MeV proton in pyrolytic graphite (ρ = 2.2 g/cm^3) is

$$dE/dz = 2.1 \text{ MeV-cm}^2/(\text{g-p}) \times 2.2 \text{ g/cm}^3 = 4.62 \text{ MeV/(cm-p)} \text{ (see Ref. 4)} .$$

Assuming an average beam current of 1 mA, we have

$$I = 10^{-3} \text{ C/s} \times (1.6 \times 10^{-19})^{-1} \text{ p/C} = 6.25 \times 10^{15} \text{ p/s} .$$

Thus, the total power loss per centimeter is

$$dP/dz = dE/dz \times I = 4.62 \text{ MeV/(cm-p)} \times 6.25 \times 10^{15} \text{ p/s} \times 1.6 \times 10^{-13} \text{ J/MeV}$$

$$= 4.62 \times 10^{3} \text{ W/cm} .$$

For an 8-cm-thick target,

$$P = 4.62 \times 10^{3} \text{ W/cm} \times 8 \text{ cm} = 3.74 \times 10^{4} \text{ W} .$$

This estimate is slightly low as dE/dz increases with decreasing proton energy. This decrease is 0.066 MeV/cm over the range of 40 MeV/cm × 8 cm, near 800 MeV. This is roughly 1% of the energy loss and is accounted for by rounding up to 40 kW.

IV. TSAAS

TSAAS is a computer code that is capable of performing transient or steady-state thermal-stress analyses of axisymmetric solids. The version we used, P-TSAAS, analyzes planar materials.

The chief inputs to the code are the target geometry; a logical map of the target; material properties; and pressure, shear, flux, or temperature boundary conditions. The code then approximates the continuous material by a set of discrete nodes, the number and general location of the nodes being specified by the coordinates of the line segments defining the logical map. The temperatures and stresses are computed numerically at the nodes. Linear interpolation between nodes gives a continuous distribution of te...peratures and stresses.

The first mesh (map of nodes) used in the early stages of the analysis is shown in Fig. 5. The nodal points are numbered consecutively from left to right, starting at the beam axis (Nodal Point 1) and moving up. When the Gaussian nature of the beam was treated, the logical map shown in Fig. 6 was fed into the code along with the target geometry to give the mesh shown in Fig. 7. The greater number of nodes in the region near the beam spot was designed to give more precision to the calculations in the region of maximum temperatures and stresses.*

V. FIRST ELEMENTARY ANALYSIS

The main objectives of the first target analysis were to provide a "ball-park" estimate of the temperatures and stresses and to ascertain that the program was running properly. Comparison of the results of this analysis with those of a similar thermal analysis performed by L. O Lindquist and P. Varghese, using the computer code TRUMP,[5] showed similar results.

*As will be shown in Sec. V, the maximum temperatures and stresses lie within the first centimeter of the beam axis.

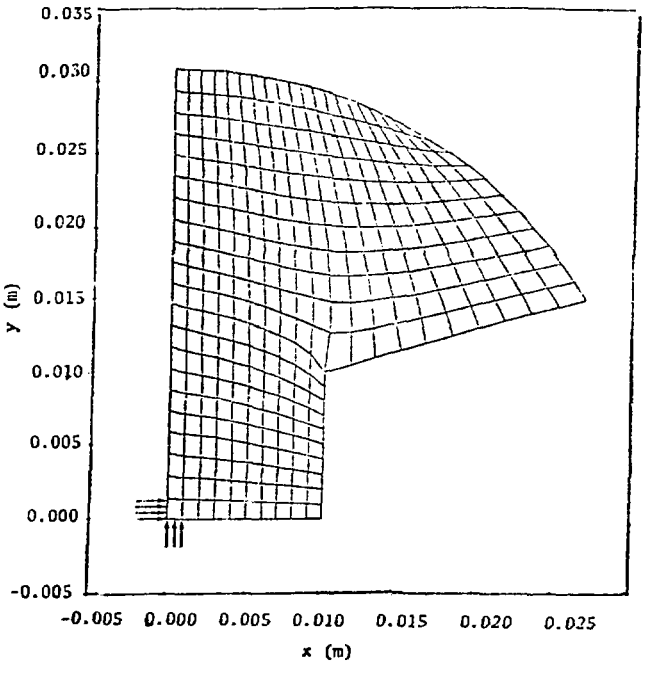

Fig. 5.
Elementary target mesh.

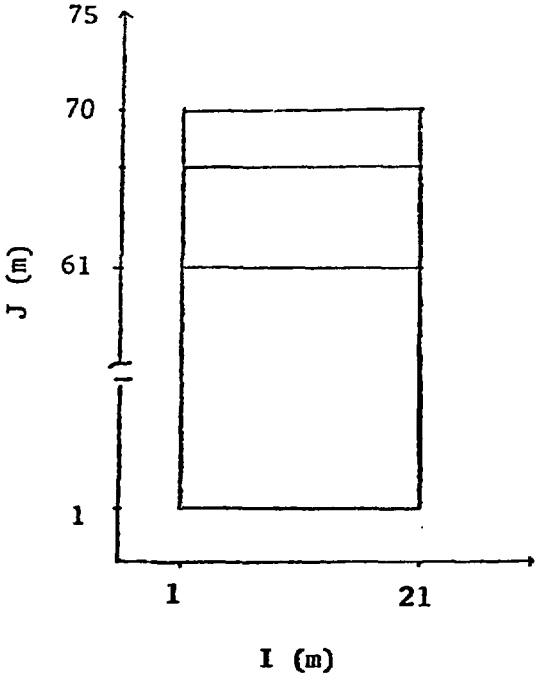

Fig. 6
Logical map of target geometry.

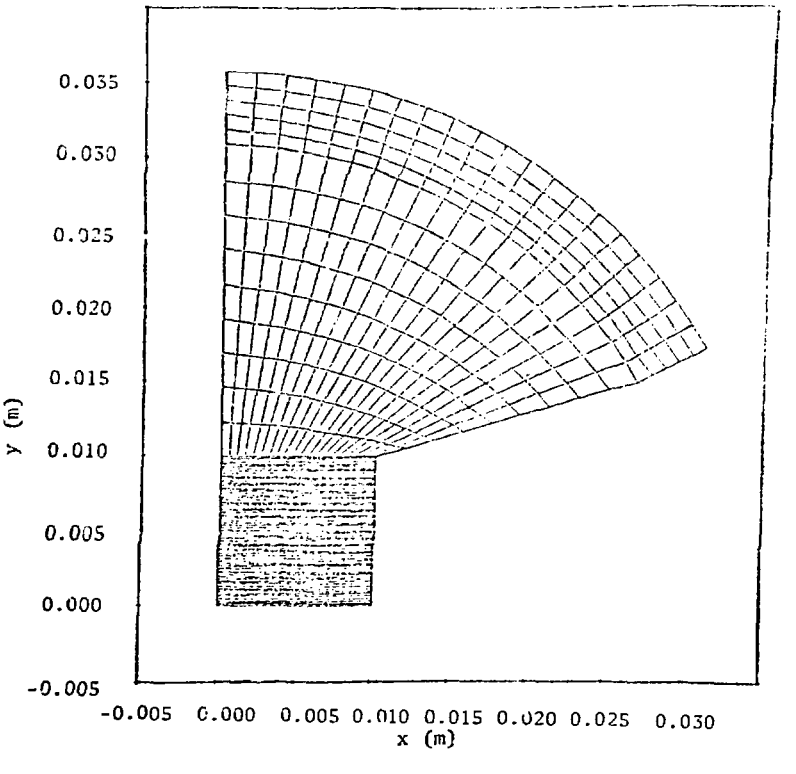

Fig. 7.
Target mesh for Gaussian heating.

Two simplifying assumptions were made for the analysis. First, the target properties, mechanical and thermal, were assumed independent of temperature.* The values assigned to the temperature-independent properties are listed in Table II. Secondly, the power dissipated in the target was treated as an energy flux incident on the sides of the target (see arrows in Fig. 4). The beam was assumed to have a circular cross section with a radius of 1 mm. The flux incident on two sides, each of dimensions 0.001 by 0.08 m, sufficient to deliver 10 kW is

$$10 \text{ kW} \div (2 \times 0.001 \times 0.08) \text{ m}^2 = 6.25 \times 10^7 \text{ W/m}^2 .$$

An error in meshing resulted in 20% greater power deposition than intended. For the first run, this was not considered important enough to rerun the program.

Fixing the circular heat sink boundary at 373 K, we obtained the following results:

Maximum Temperature	= 1652 K
Maximum Stress in Compression	= 0.18×10^8 N/m^2
**Maximum Stress in Tension	= 0.15×10^8 N/m^2 .

Figures 8(a)-(c) are computer-generated contour plots for the temperature and stress distributions of this first analysis. Comparison of these values with the sublimation temperature and ultimate tensile and compressional strengths of graphite indicates no failure of the target. The evaporation rate of graphite at the maximum temperature (Fig. 1) is negligible.

One of the options available with TSAAS is the ability to assign an internal heat-generation rate to a block of nodes. This has units of power per unit mass and is homogeneous over the designated block.

*The Appendix presents graphs of various material properties as a function of temperature. For all except the thermal conductivity, this is not a bad assumption.

**In all cases, the maximum compressional stress occurred at Nodal Point 1, the beam axis. The maximum tensile stress occurred at the next-to-last nodal point in the first row (y = 0).

TABLE II

PHYSICAL PROPERTIES OF PYROLYTIC GRAPHITE

Property	Value
Density (kg/m^3)	2.2×10^3
Elastic Modulus (N/m^2)	3.1×10^{10}
Poisson's Ratio	0.24
Coefficient of Thermal Expansion (K^{-1})	2.1×10^{-6}
Ratio Plastic to Elastic Modulus	1
Thermal Conductivity (W/mK)	390
Heat Capacity (J/kgK)	970

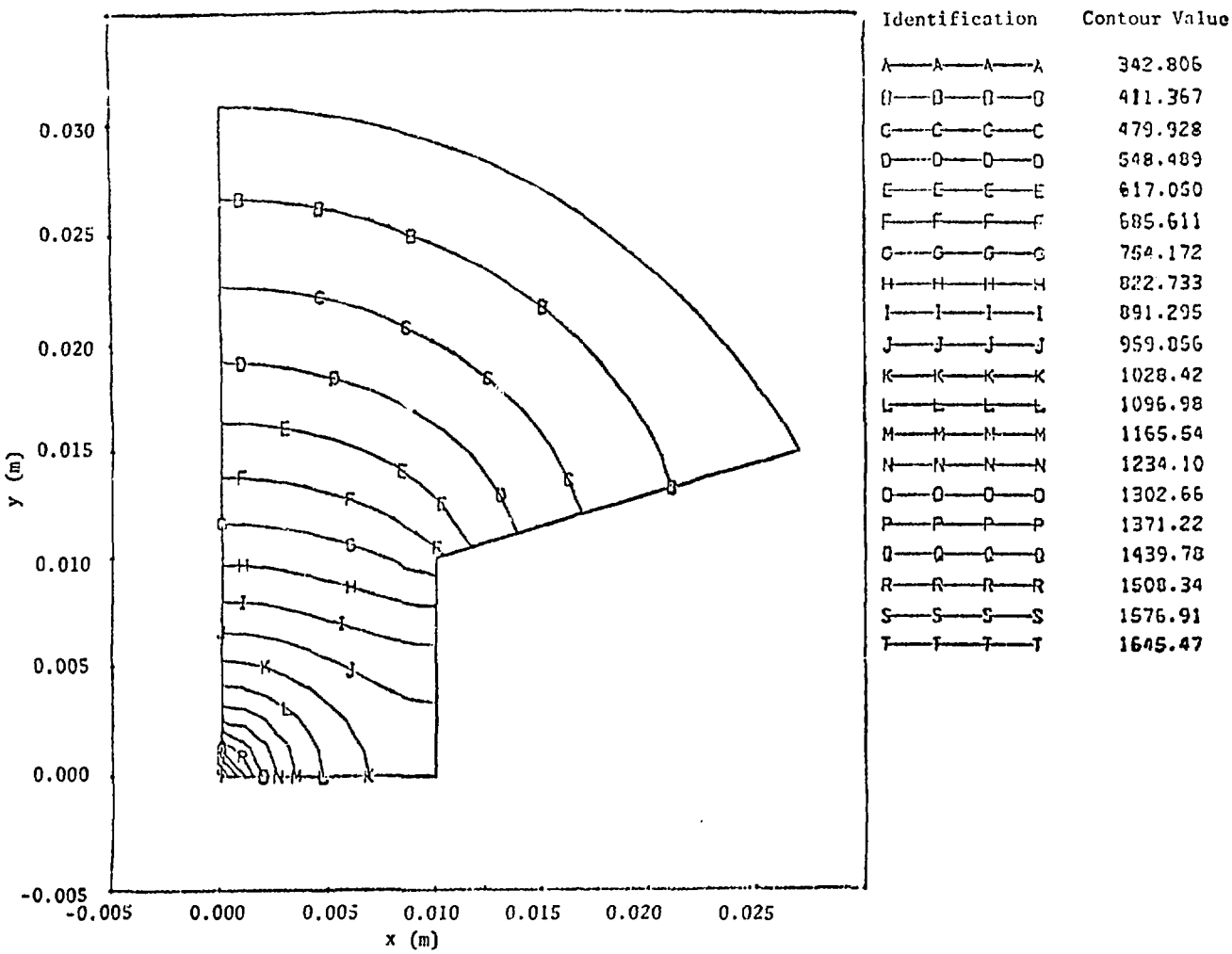

Fig. 8(a).
Temperature contour plots from first analysis (flux boundary conditions, temperature-independent physical properties).

In the second run, the flux boundary conditions were replaced by a 0.001- by 0.001- by 0.08-m block, which generated heat at a rate of 5.68×10^7 W/kg.* Keeping the other properties the same as in the previous run, we found [see Figs. 9(a)-(c)].**

Maximum Temperature = 1831 K

Maximum Stress in Compression = 0.24×10^8 N/m^2

Maximum Stress in Tension = 0.2×10^8 N/m^2 .

*10 kW/(0.001 by 0.001 by 0.08) m^3 $\times$ 1/(2.2 $\times$ 10^3) kg/m^3 = 5.68×10^7 W/kg.

**The mesh used in this calculation is shown in Fig. 7.

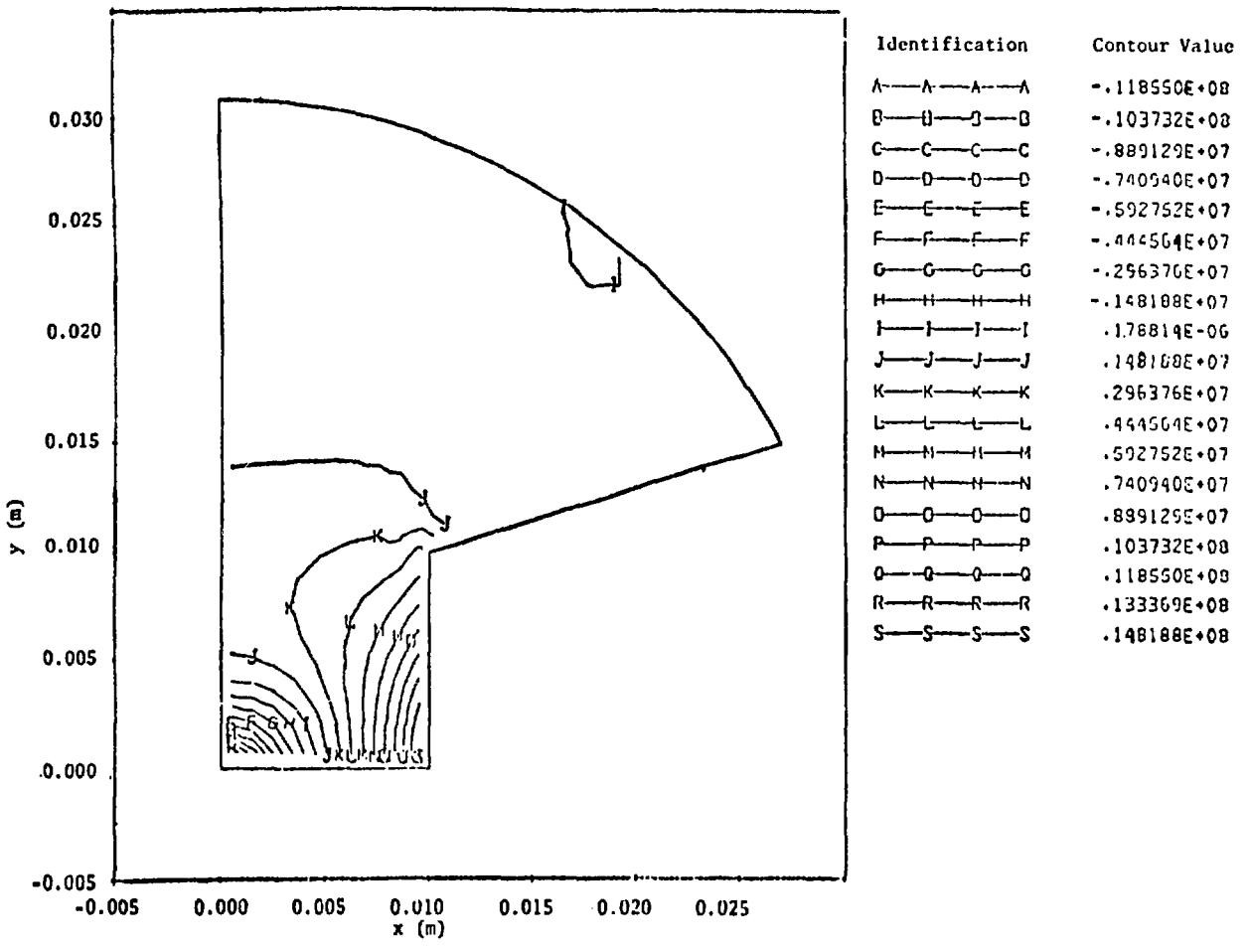

Fig. 8(b).
Maximum stress contour plots from first analysis.

VI. GAUSSIAN BEAM

Until now, the beam has been assumed to be circular in the cross section, with a constant current density. In reality, the LAMPF proton beam is Gaussian in both x and y (perpendicular to the beam axis). To simulate the Gaussian nature of the beam current density, various blocks of nodes were assigned internal heat-generation rates that varied in an approximately two-dimensional Gaussian fashion. With other physical properties fixed at their previous values, this semi-Gaussian power distribution gave a hot-spot temperature several hundred degrees lower and stresses slightly below those of the previous run.

Assuming a Gaussian current distribution in x and y, an equation for the power loss distribution in the graphite is

$$\frac{dP}{dV} = \frac{\frac{dE}{dz} \times I}{2\pi\sigma_x\sigma_y} \; e^{-\frac{1}{2}\left(\frac{x^2}{\sigma_x^2} + \frac{y^2}{\sigma_y^2}\right)} ,$$

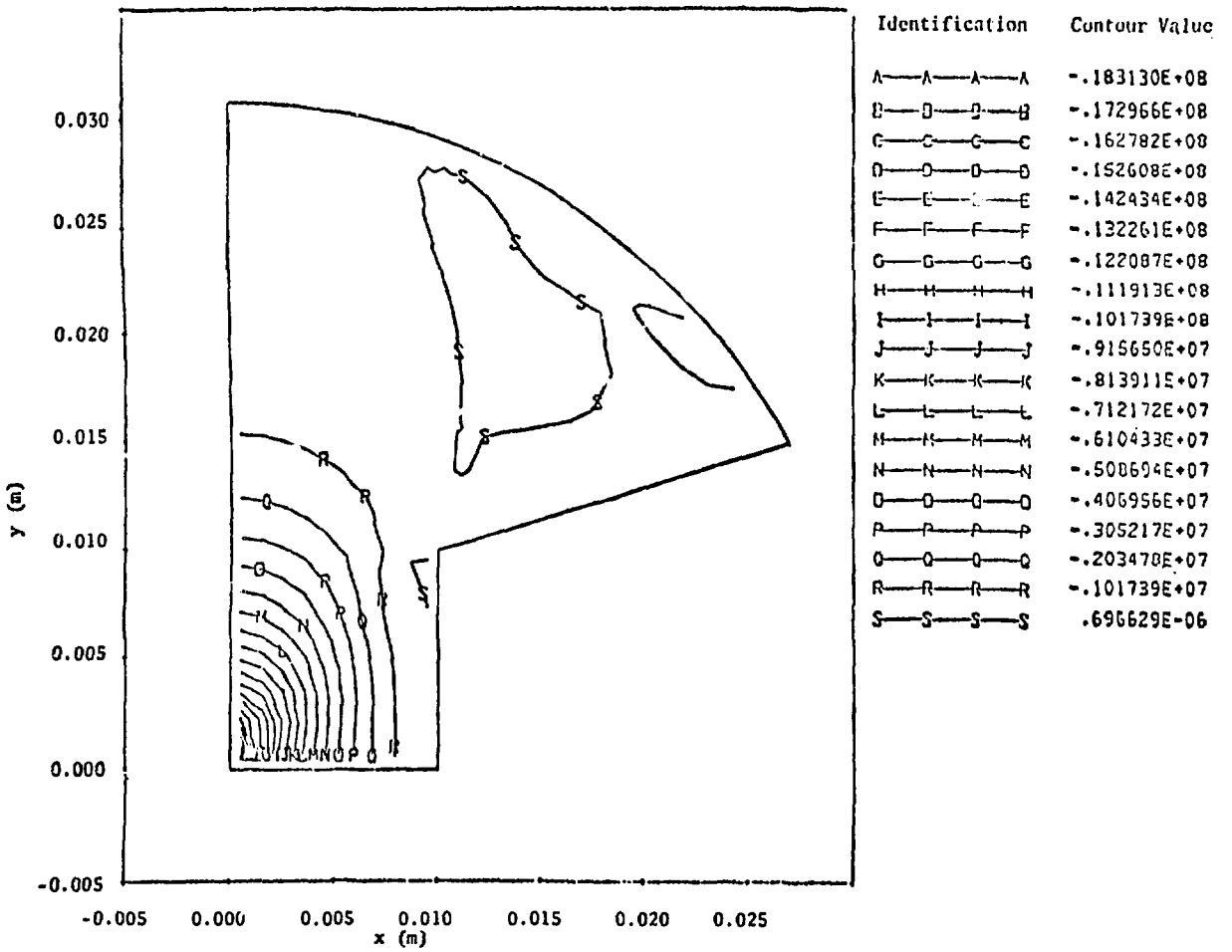

Fig. 8(c).
Minimum stress contour plots from first analysis.

where x and y are the displacements from beam center and σ_x and σ_y are the standard deviations of the beam current density in x and y. From the assumption that dE/dz = const = 4.62 MeV/cm, the total power deposited in a given region of the target ($0 \le z \le 0.08$ m, $y_0 \le y \le y_1$, $x_0 \le x \le x_1$) is

$$P = \int_{x_0}^{x_1} \int_{y_0}^{y_1} \int_{0}^{0.08} \frac{dE}{dz} \times I \; \frac{e^{-\frac{1}{2}\left(\frac{x^2}{\sigma_x^2} + \frac{y^2}{\sigma_y^2}\right)}}{2\pi\sigma_x\sigma_y} \, dz\,dy\,dx$$

$$= 40 \text{ kW} \int_{x_0}^{x_1} \int_{y_0}^{y_1} \frac{e^{-\frac{1}{2}\left(\frac{x^2}{\sigma_x^2} + \frac{y^2}{\sigma_y^2}\right)}}{2\pi\sigma_x\sigma_y} \, dy\,dx \quad .$$

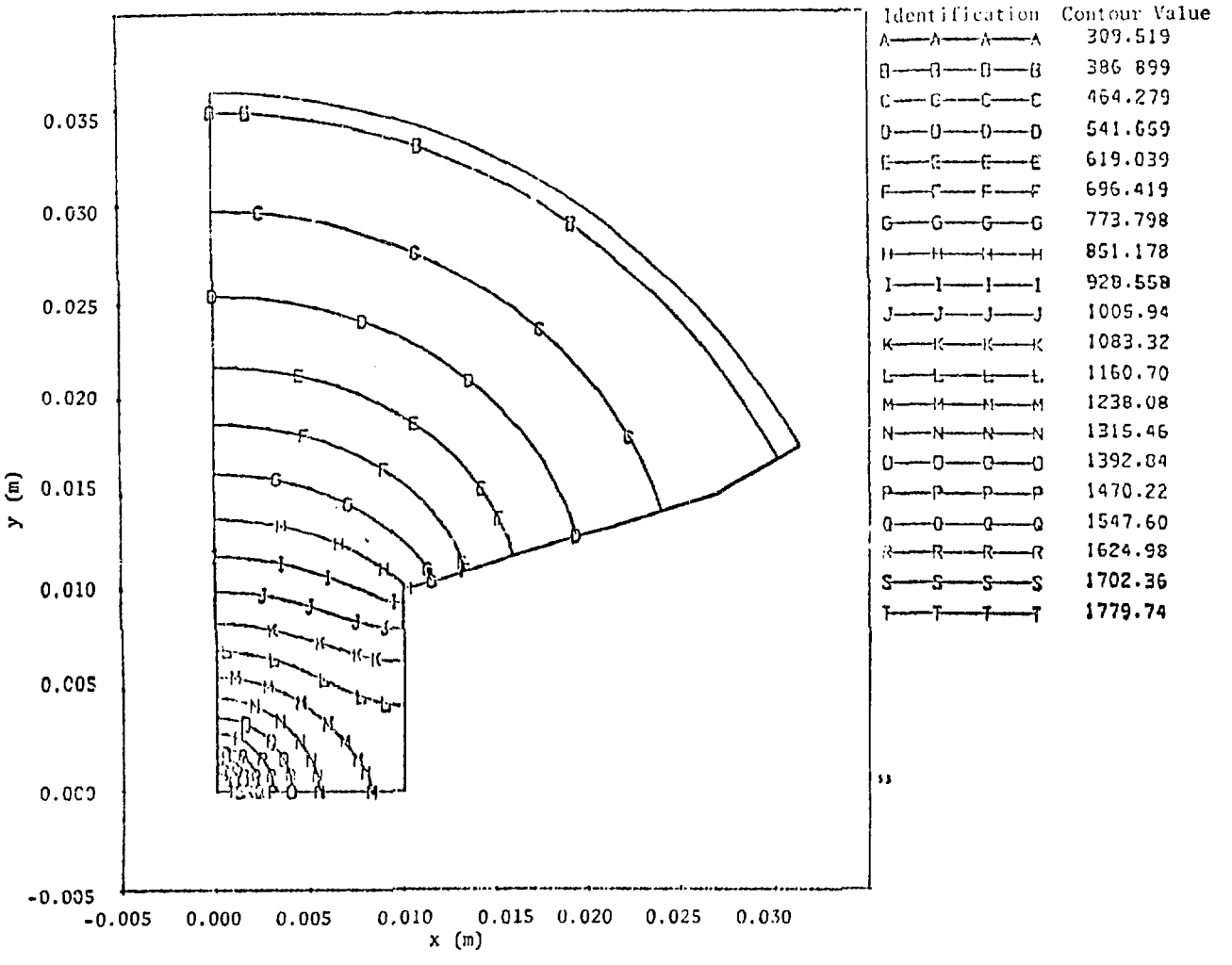

Fig. 9(a).
Temperature contour plots (non-Gaussian internal heat-generation rate, fixed physical properties).

Since 99.48% of the beam is contained within the region ($3\sigma_x \le x \le 3\sigma_x$ and $3\sigma_y \le y \le 3\sigma_y$), the amount of power dissipated outside this region was neglected. The region of power deposition in the quarter section analyzed was divided into nine sections, each of dimensions σ_x by σ_y by 0.08 m.

The minimum beam parameters given for the LAMPF proton beam are

$$2\sigma_x = 3 \text{ mm}$$

$$2\sigma_y = 1 \text{ mm}$$

on Line A. These quantities are the results of measurements of current LAMPF beam profiles near Target Cell A-1, the smallest available profiles on Line A. The minimum beam profile should produce the highest temperatures and stresses in the target material. The results obtained using these parameters thus constitute an upper limit for temperatures and stresses to be

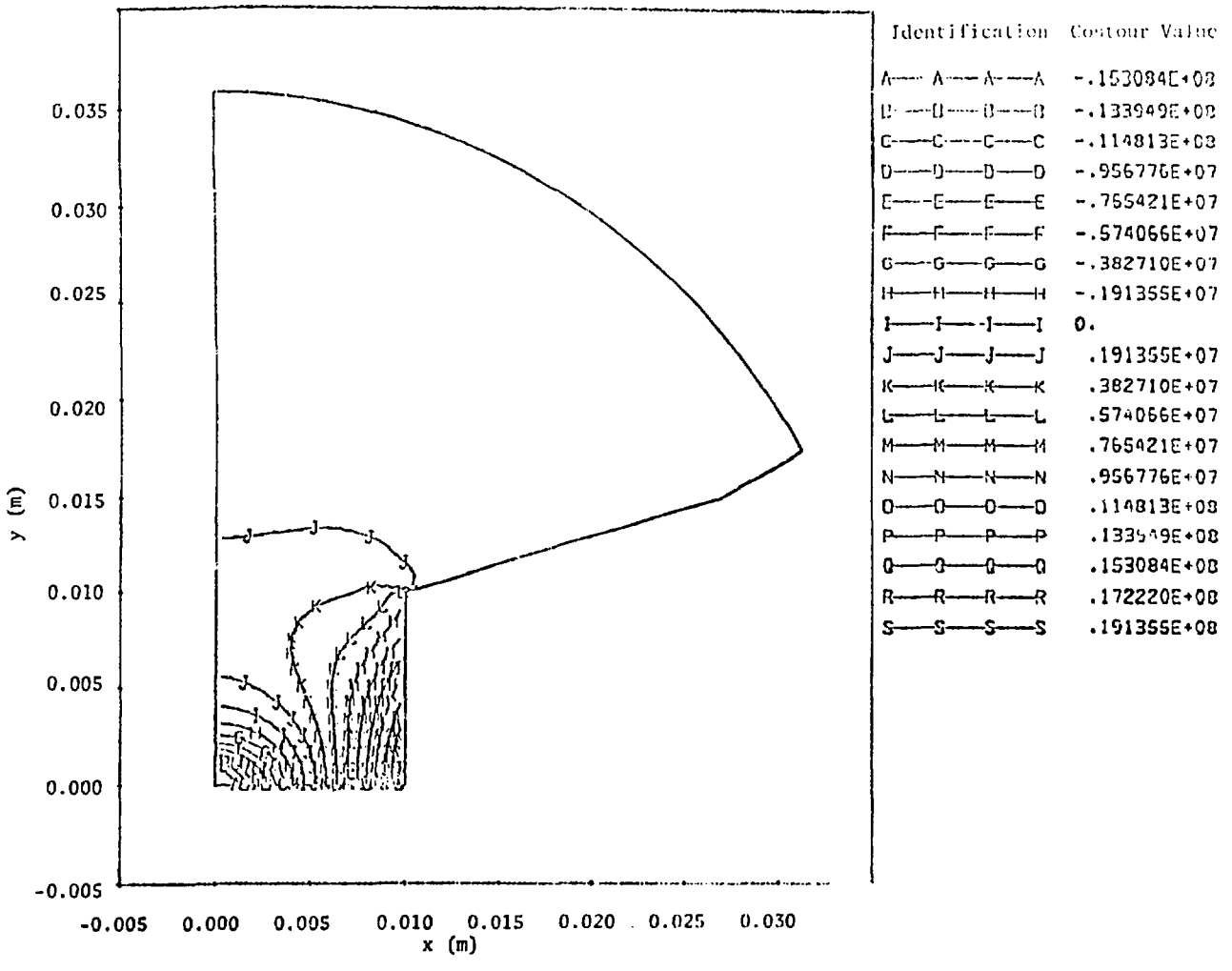

Fig. 9(b).
Maximum stress contours.

encountered in any Line A target position (A-1, A-2, ..., A-6). Table III gives the total power loss per unit mass in each of the nine heated regions using the above values of σ_x and σ_y.

The maximum temperatures and stresses obtained using this semi-Gaussian power distribution and the same material properties used in the previous runs are given below.

Maximum Temperature = 1296 K

Maximum Stress in Compression = 0.12×10^8 N/m^2

Maximum Stress in Tension = 0.13×10^8 N/m^2 .

Figures 10(a)-(c) give the temperature and stress contours for this calculation. The lower temperatures and stresses are to be expected with a Gaussian distribution.

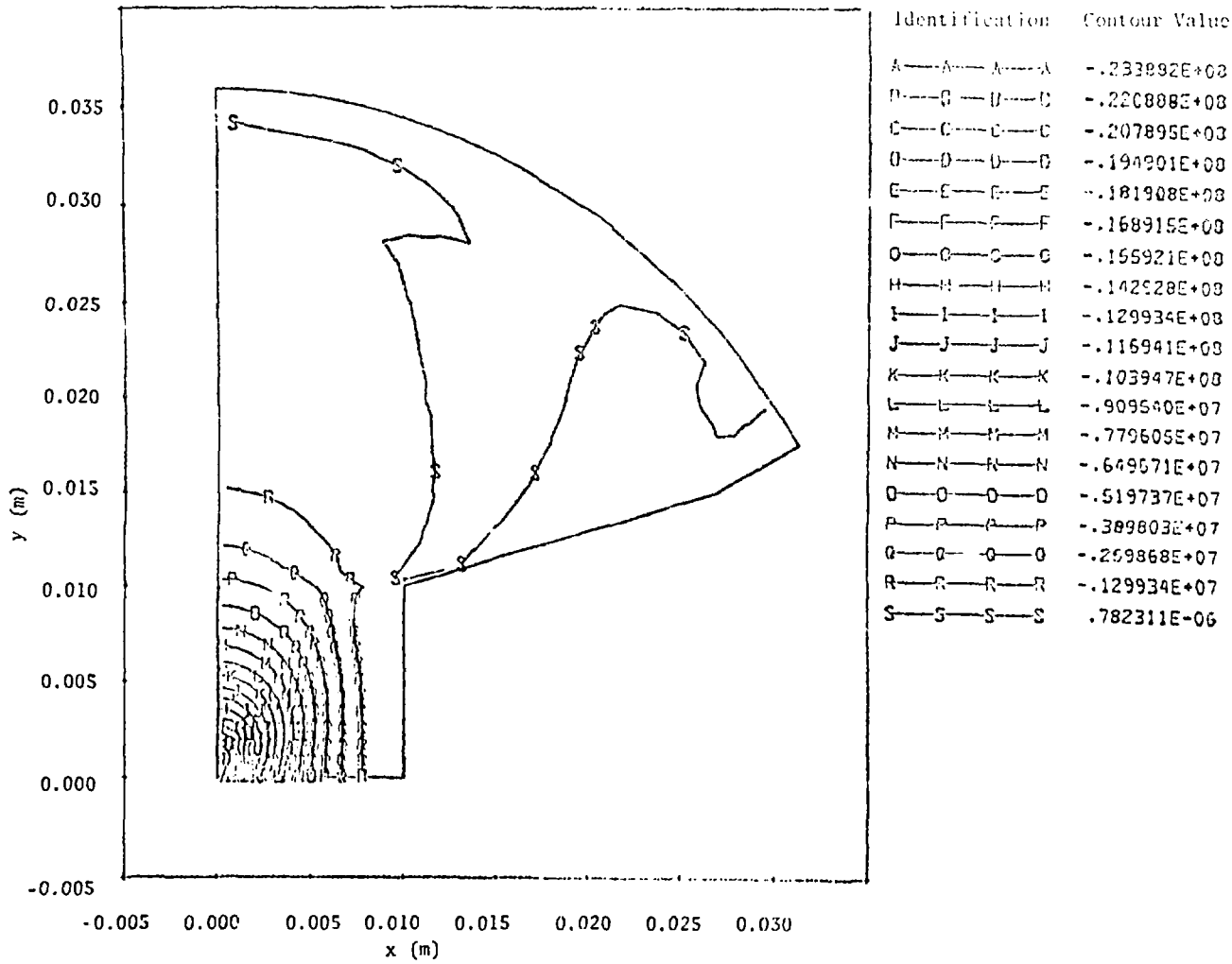

Fig. 9(c).
Minimum stress contours.

VII. TEMPERATURE DEPENDENCE OF PHYSICAL PROPERTIES

In the final step of the analysis, the temperature dependence of the thermophysical properties was taken into account. Given a maximum of six input values, TSAAS will interpolate between the values to generate a piecewise linear function that describes the given property as a function of temperature.

The only physical property of pyrolytic graphite that varies significantly over the temperature range considered (350-1500 K) is the thermal conductivity; its value drops from 1690 W/mK at 350 K to 340 W/mK at 1500 K. After running the program several times and choosing varying points along the conductivity curve, the thermal conductivity values used were those at the following temperatures: 350, 400, 500, 600, 700, and 800 K. These gave the best fit to the thermal conductivity curve while including all temperatures encountered in the steady-state temperature calculation. With the Gaussian heat distribution and the variable thermal conductivity, we computed

TABLE III

TWO-DIMENSIONAL GAUSSIAN POWER DISTRIBUTION IN TARGET

General Form: $P_{region} = 40\ KW \int_{x_1}^{x_2} \int_{y_1}^{y_2} G\ dxdy$,

where $G = \dfrac{e^{-\frac{1}{2}\left(\frac{x}{\sigma x^2} + \frac{y^2}{\sigma y^2}\right)}}{2\pi\sigma_x\sigma_y}$.

Region	x_1	x_2	y_1	y_2	Power (MW/kg)
1	0_x	σ_x	0	σ_y	35.3
2	σ_x	$2\sigma_x$	0	σ_y	14.0
3	$2\sigma_x$	$3\sigma_x$	0	σ_y	2.4
4	0	σ_x	σ_y	$2\sigma_y$	1.4
5	σ_x	$2\sigma_x$	σ_y	$2\sigma_y$	5.6
6	$2\sigma_x$	$3\sigma_x$	σ_y	$2\sigma_y$	0.94
7	0	σ_x	$2\sigma_y$	$3\sigma_y$	7.4
8	σ_x	$2\sigma_x$	$2\sigma_y$	$3\sigma_y$	0.94
9	$2\sigma_x$	$3\sigma_x$	$2\sigma_y$	$3\sigma_y$	0.15

Maximum Temperature = 701 K

Maximum Stress in Compression = 0.53×10^7 N/m^2

Maximum Stress in Tension = 0.49×10^7 N/m^2 .

Temperature and stress contours are shown in Figs. 11(a)-(c). Using a single thermal conductivity of 390 W/mK (taken from a table, not a graph) for the previous case gave us somewhat misleading results (1296 K and 0.13×10^8 N/m^2). To test the effect of the variable thermal conductivity on previous results, the Gaussian heat distribution was removed and replaced by the 0.001- by 0.001- by 0.08-m block generating heat at a constant rate. The results are as follows:

Maximum Temperature = 722 K

Maximum Stress in Compression = 0.67×10^7 N/m^2

Maximum Stress in Tension = 47×10^7 N/m^2 .

Figures 12(a)-(c) show the temperature and stress plots for this case.

As a final check on these results, Figs. 13 and 14 give the plots of the x and y stresses as a function of displacement from the beam axis. The Gaussian nature of the plots and the size of the full

UNIVERSITY OF CALIFORNIA
LOS ALAMOS SCIENTIFIC LABORATORY
(CONTRACT W-7405-ENG-36)
P.O. BOX 1663
LOS ALAMOS, NEW MEXICO 87545

IN REPLY
REFER TO:
MAIL STOP:

January 5, 1978

To: Holders of LA-6936-MS

Please make changes to Table III, page 14, as follows:

Last column, fourth number down reads 1.4. Change to 14.0.
Last column, seventh number down reads 7.4. Change to 2.4.

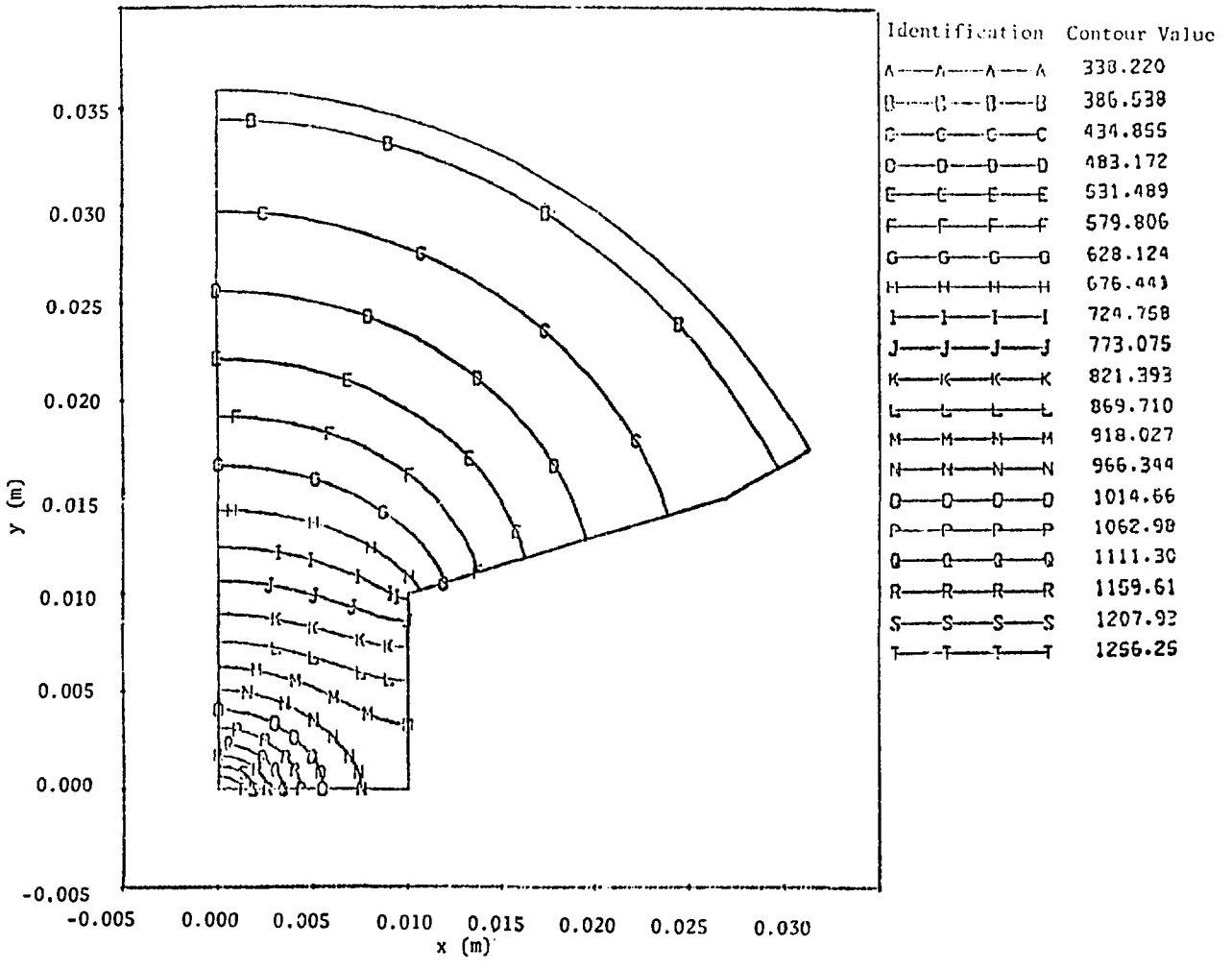

Fig. 10(a).
Temperature contours (non-Gaussian internal heat-generation rate, fixed physical properties).

width at half maxima (several times greater than those of the power distribution) indicate that the program gave realistic results.*

The maximum steady-state temperatures and stresses, in all cases, from the harshest and the most unrealistic to the most realistic set of given boundary conditions and material properties, are significantly below the maximum capabilities of pyrolytic graphite.

VIII. WATER-COOLED COPPER LAYER BONDED TO TARGET

The other target configuration considered in this report is a variation on the model that was previously analyzed. It was suggested that a copper plate be bonded to the pyrolytic graphite so the homogeneous properties of copper could be used for heat removal from the target. The model

*FWHM = 2.3 σ for a normal distribution.

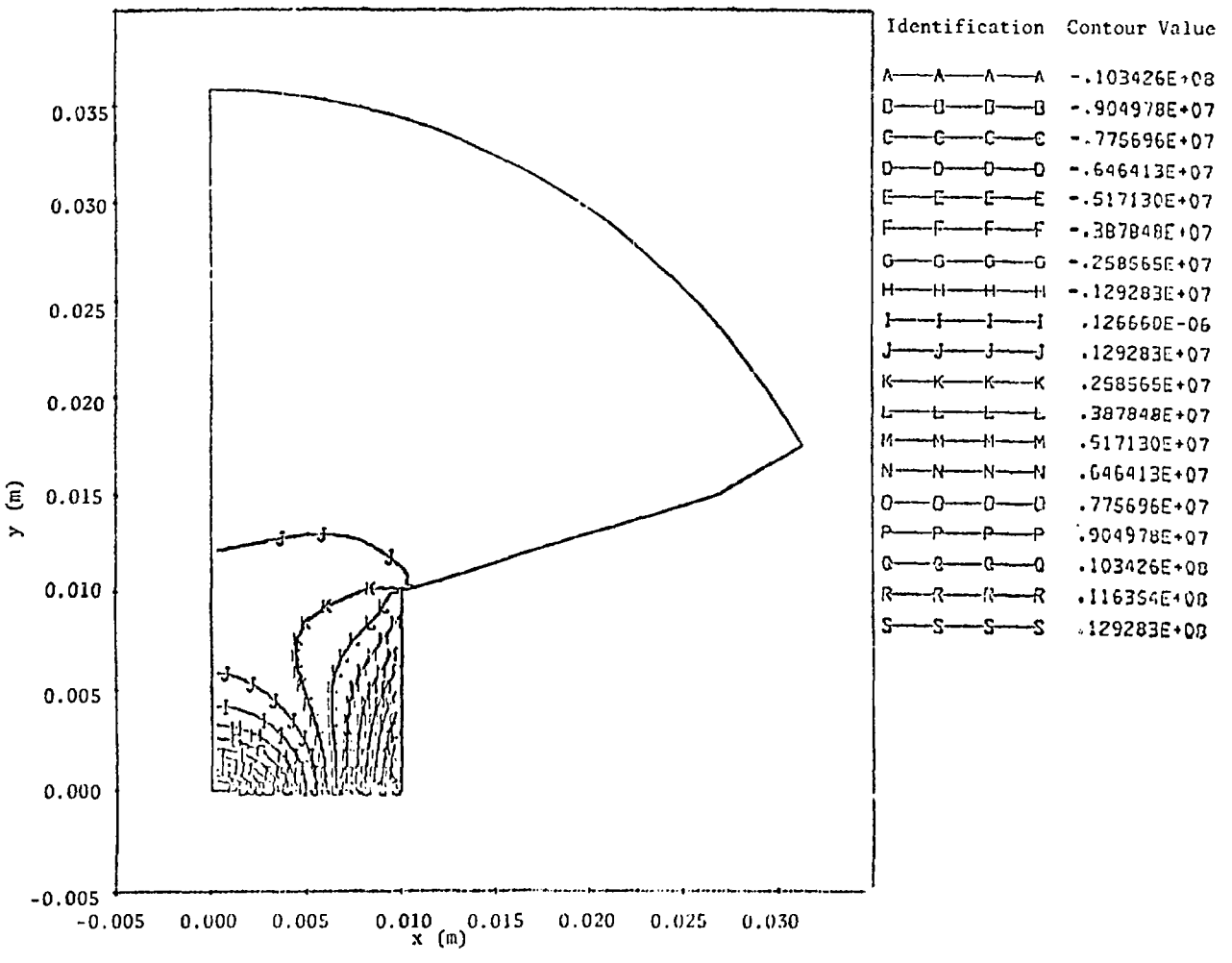

Fig. 10(b).
Maximum stress contours.

for this is shown in Fig. 3. Again, the target is I-beam-shaped and the circular bond provides an isothermal heat-transfer interface. Water flows through holes that are drilled in the copper parallel to the beam. The holes are uniformly spaced, 2 to 5 mm above the material interface.

The stresses in the direction of the beam are neglected for the same reasons as before. The temperature gradient in this direction is negligible, and the physical properties of pyrolytic graphite necessary to obtain realistic numbers are unknown (principally, the modulus of elasticity). The coefficient of thermal expansion of pyrolytic graphite perpendicular to the structural plane is 60% greater than that of copper while the coefficient of thermal expansion of pyrolytic graphite in the structural plane is eight times *less* than that of copper. Thus, the most important stresses along the copper-graphite interface should occur in the plane containing the a-b plane of the graphite.*

The temperature and stress calculations were carried out to evaluate the stresses in the a-b plane generated by the copper-graphite interface. This problem is identical to the previous one

*The stresses perpendicular to the a-b plane will be compressional. The compressional strength of pyrolytic graphite to the a-b planes is greater than the tensile strength in the a-b planes.

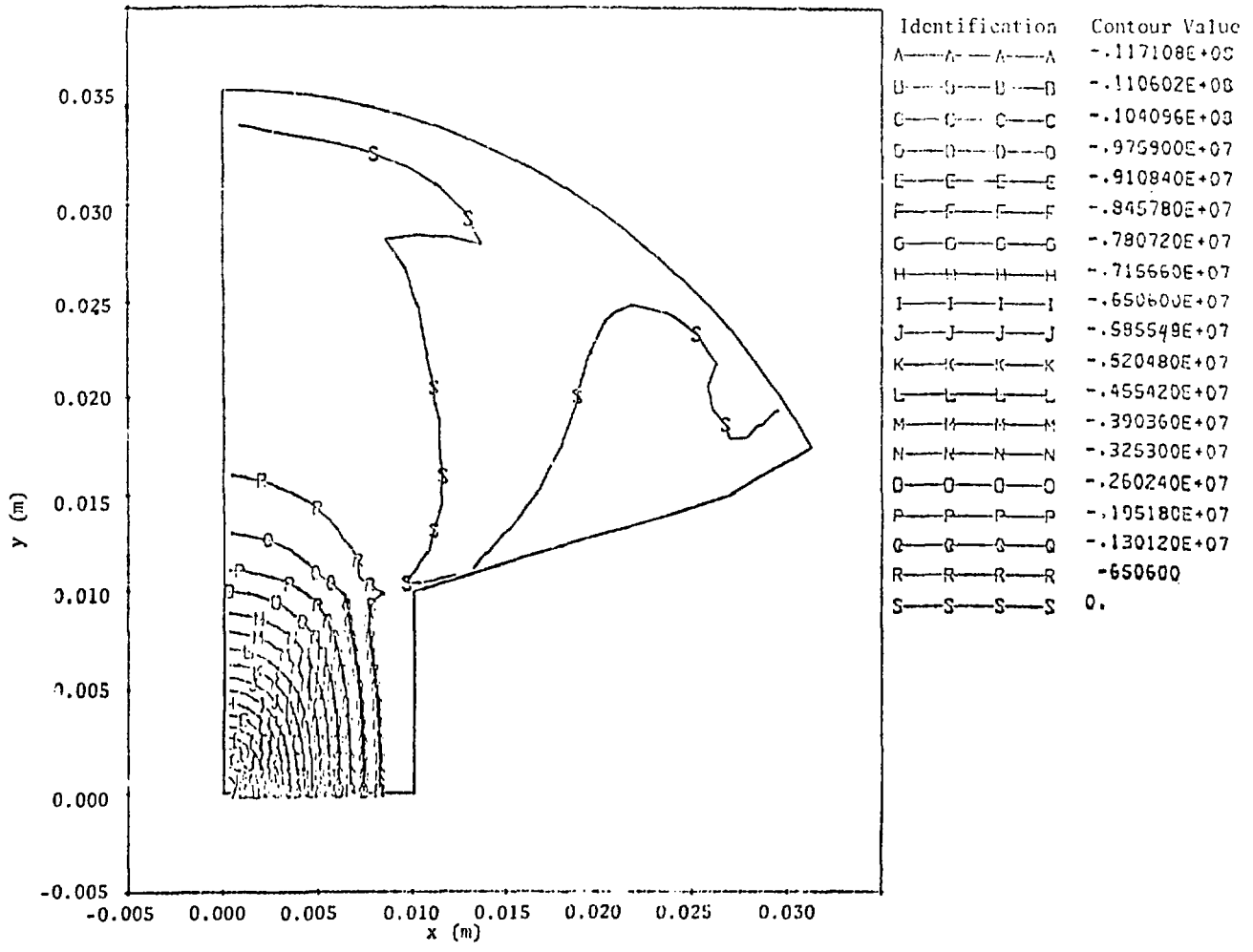

Fig. 10(c).
Minimum stress contours.

for a TSAAS analysis; indeed, the mesh in Fig. 7 was generated with the problem in mind. The only difference between this analysis and that of Sec. VII is that another material block was specified, another set of material property cards was inserted, and the width of the outer section was modified to suit the given thickness of the copper layer. Three thicknesses were considered, each corresponding to the distance between the material bond and the water tubes: 2, 3, and 5 mm. The material properties used for copper are given in Table IV.

Using the Gaussian heat distribution and variable thermal conductivity of the previous cases, we obtained temperatures and maximum stresses near the copper-graphite boundary, as shown in Table V. The graphite hot-spot temperatures and stresses (far from the copper-graphite boundary) were essentially the same as those for the case without the copper layer.

The maximum stresses due to the differing coefficients of thermal expansion of copper and pyrolytic graphite are less than the ultimate strengths of the two materials.

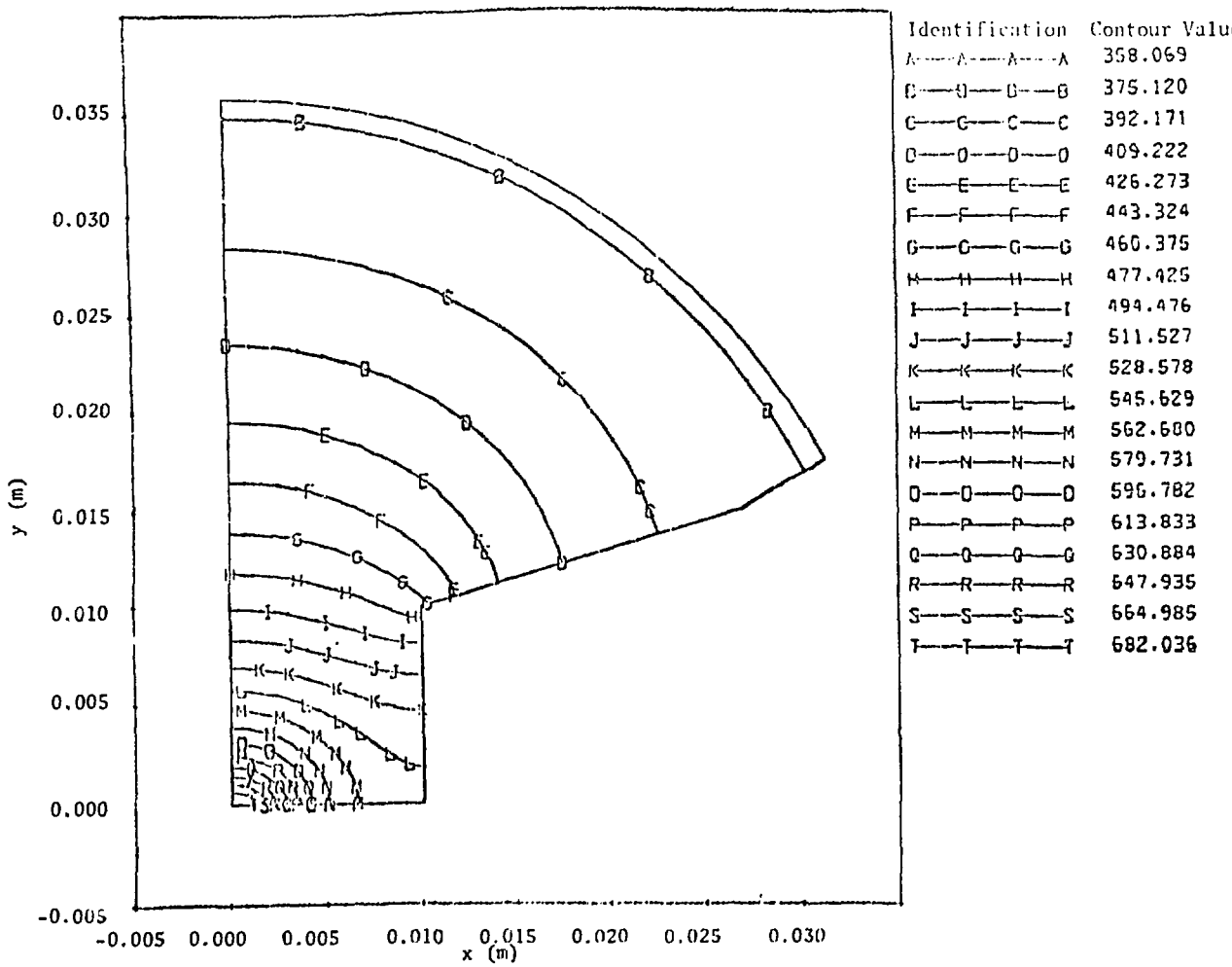

Fig. 11(a).

Temperature contours (Gaussian internal heat-generation rate, thermal conductivity a function of temperature).

TABLE IV

MATERIAL PROPERTIES OF COPPER

Property	Value
Density (kg/m^3)	8.92×10^3
Modulus of Elasticity (N/m^2)	11×10^{10}
Poisson's Ratio	0.355
Coefficient of Thermal Expansion (K^{-1})	1.76×10^{-5}
Thermal Conductivity (W/mK)	385
Heat Capacity (J/kgK)	385

Melting Point of Copper = 1456 K
Yield Strength of Copper $\simeq 3.1 \times 10^8$ N/m^2

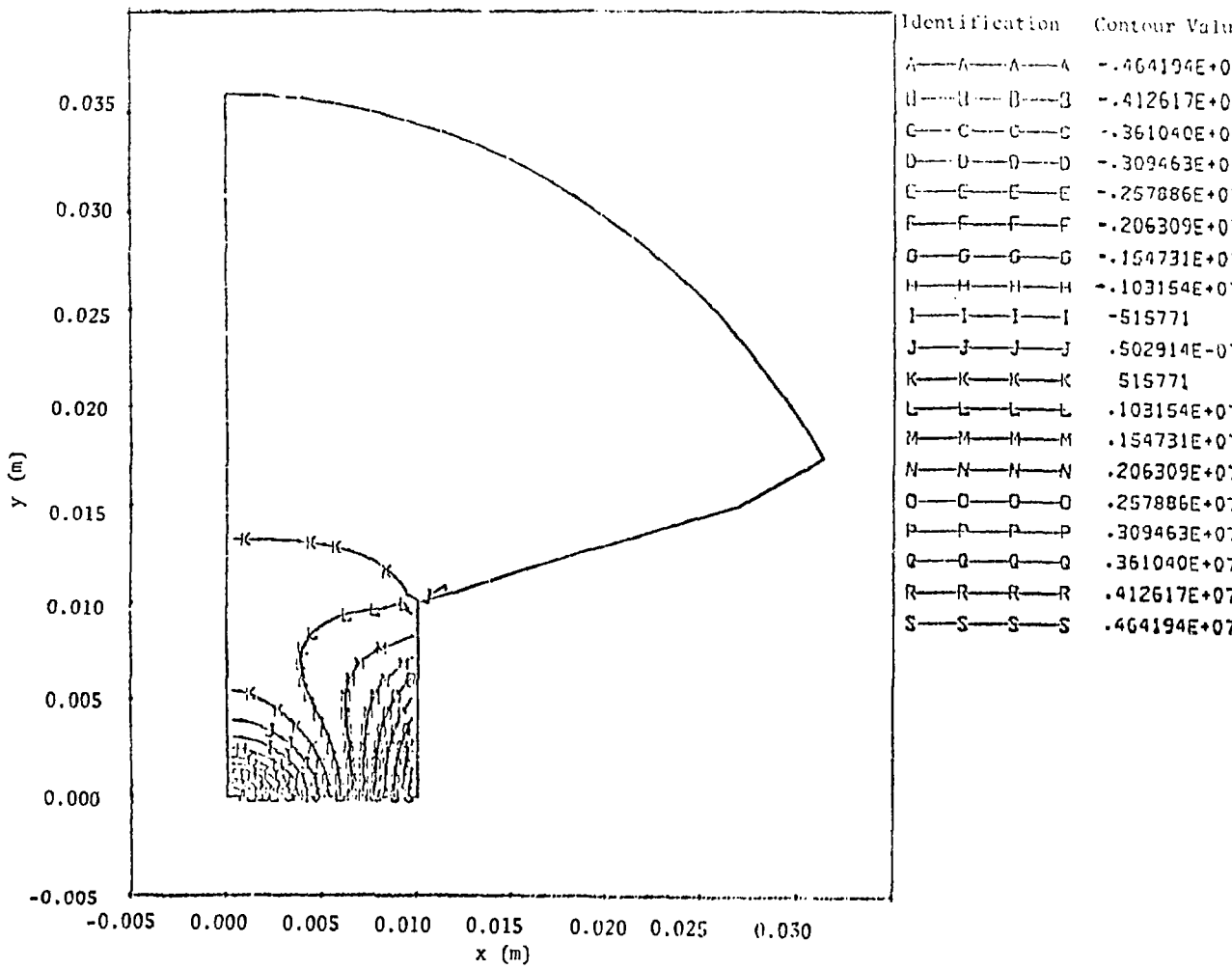

Fig. 11(b).
Maximum stress contours.

Using the Gaussian heat distribution and variable thermal conductivity of the previous cases, we obtained temperatures and maximum stresses near the copper-graphite boundary, as shown in Table V. The graphite hot-spot temperatures and stresses (far from the copper-graphite boundary) were essentially the same as those for the case without the copper layer.

The maximum stresses due to the differing coefficients of thermal expansion of copper and pyrolytic graphite are less than the ultimate strengths of the two materials.

IX. SUMMARY

Two target configurations, suitable for the LAMPF A-1, A-2, or A-5 pion production site, were analyzed for maximum thermal stresses and temperatures expected for a steady-state power deposition corresponding to the full design capabilities of the LAMPF proton accelerator. Both

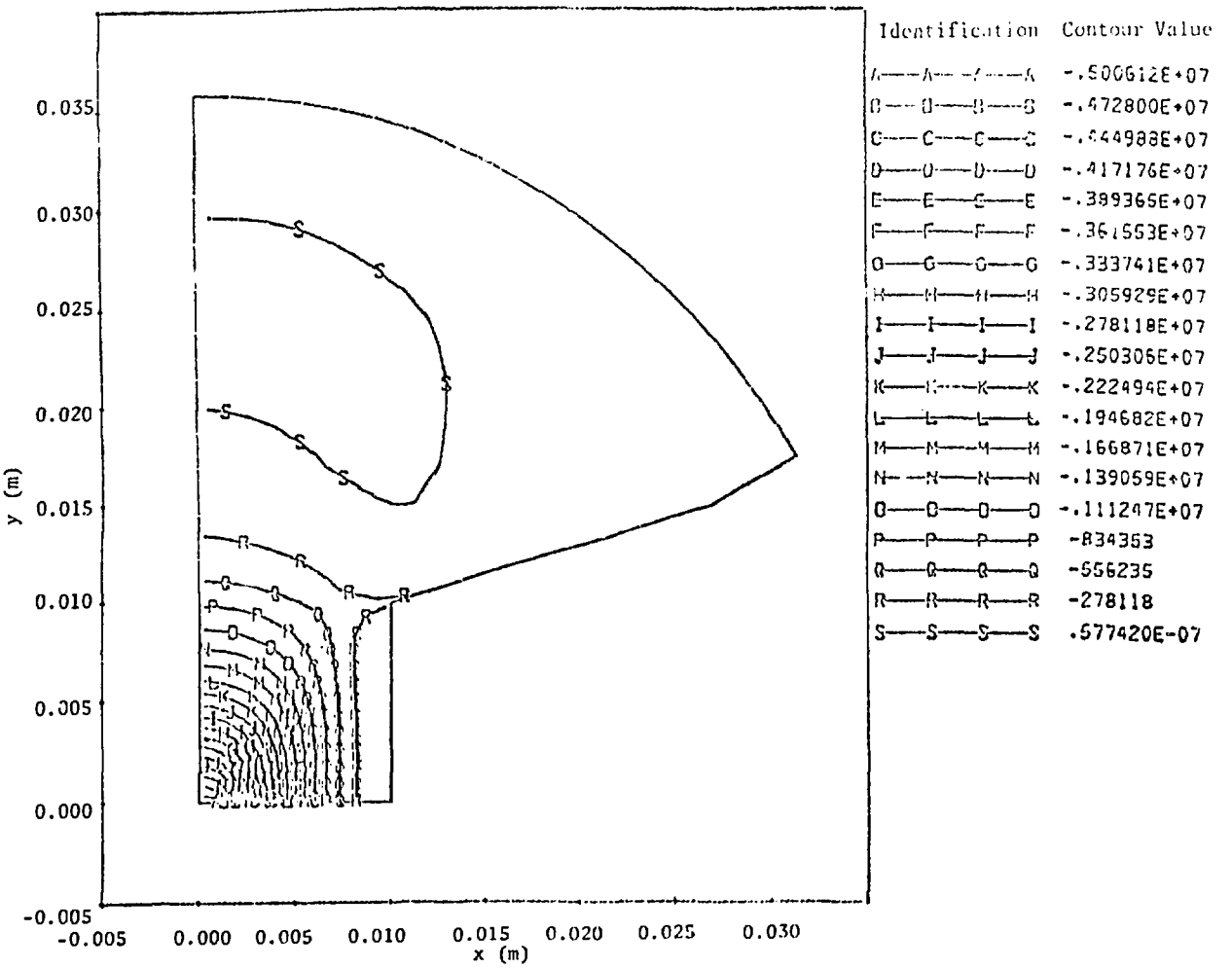

Fig. 11(c).
Minimum stress contours.

TABLE V

COMPUTER STRESSES WITH VARIED COPPER-LAYER THICKNESS

Copper Layer Thickness (mm)	Boundary Temperature (K)	Maximum Stress (N/m^2)
2	380	$^{a}0.17 \times 10^{8}$
3	400	$^{a}0.32 \times 10^{8}$
5	416	$^{a}0.61 \times 10^{8}$

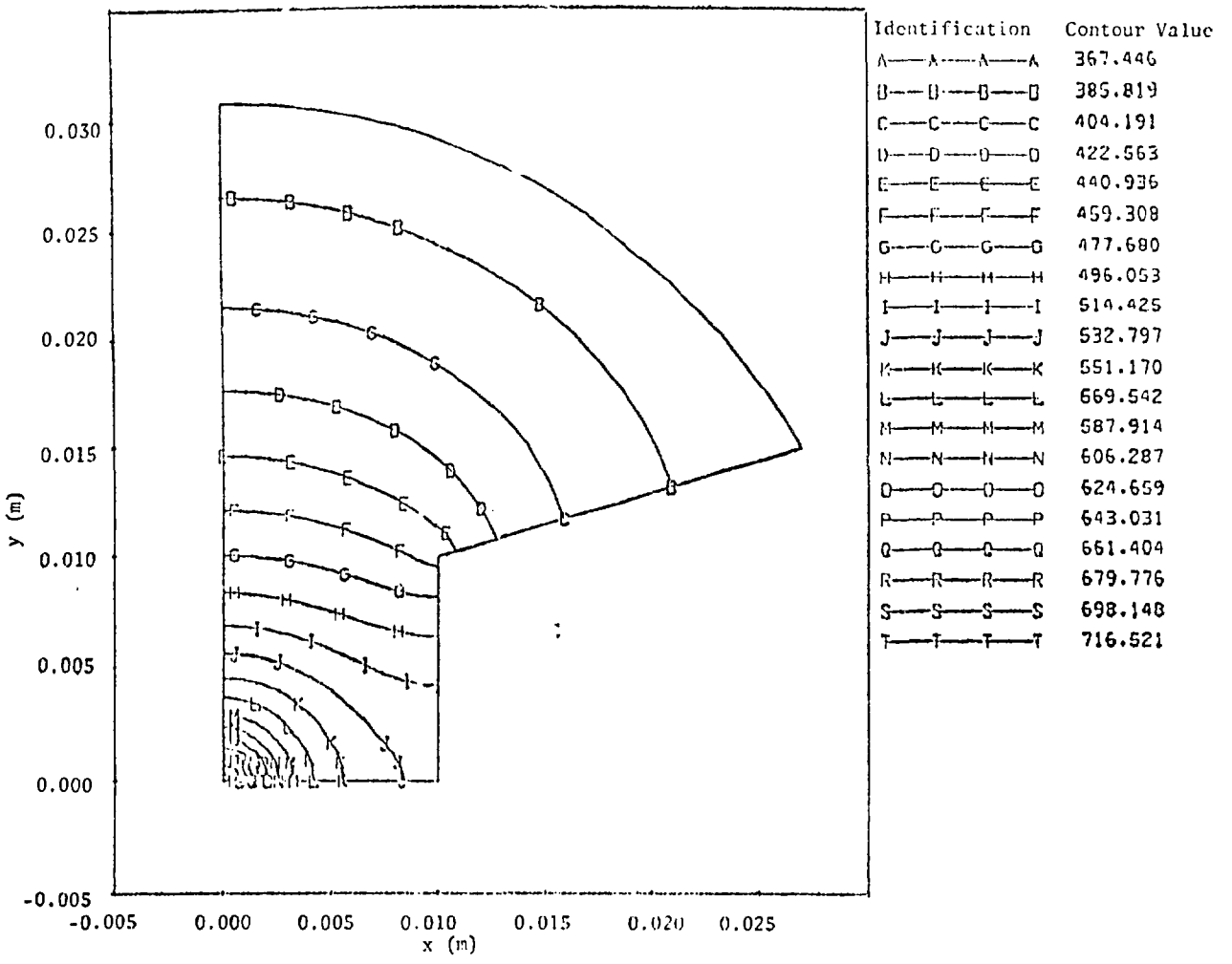

Fig. 12(a).
Temperature contours (non-Gaussian internal heat-generation rate, thermal conductivity a function of temperature).

targets were composed of pyrolytic graphite, cooled by flowing water. Both configurations were I-beam-shaped to provide minimum interference with experimental channels and minimum interference with the beam during insertion or removal. In both cases, the maximum temperatures and stresses caused by steady-state beam heating were well within the capabilities of the target materials.

ACKNOWLEDGMENTS

The authors wish to express their appreciation to Richard V. Browning (Group WX-3, LASL), for his invaluable aid in the use of TSAAS.

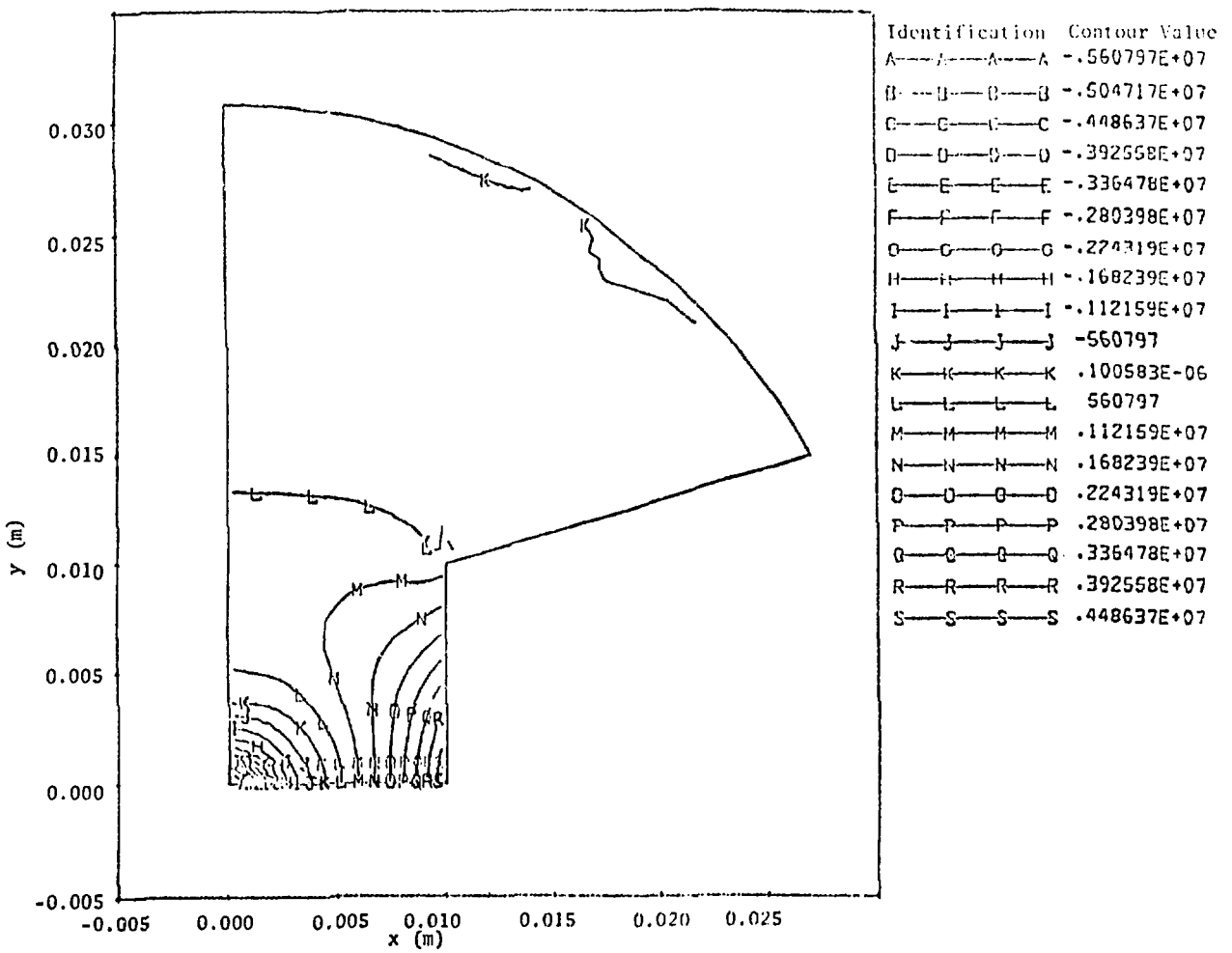

Fig. 12(b).
Maximum stress contours.

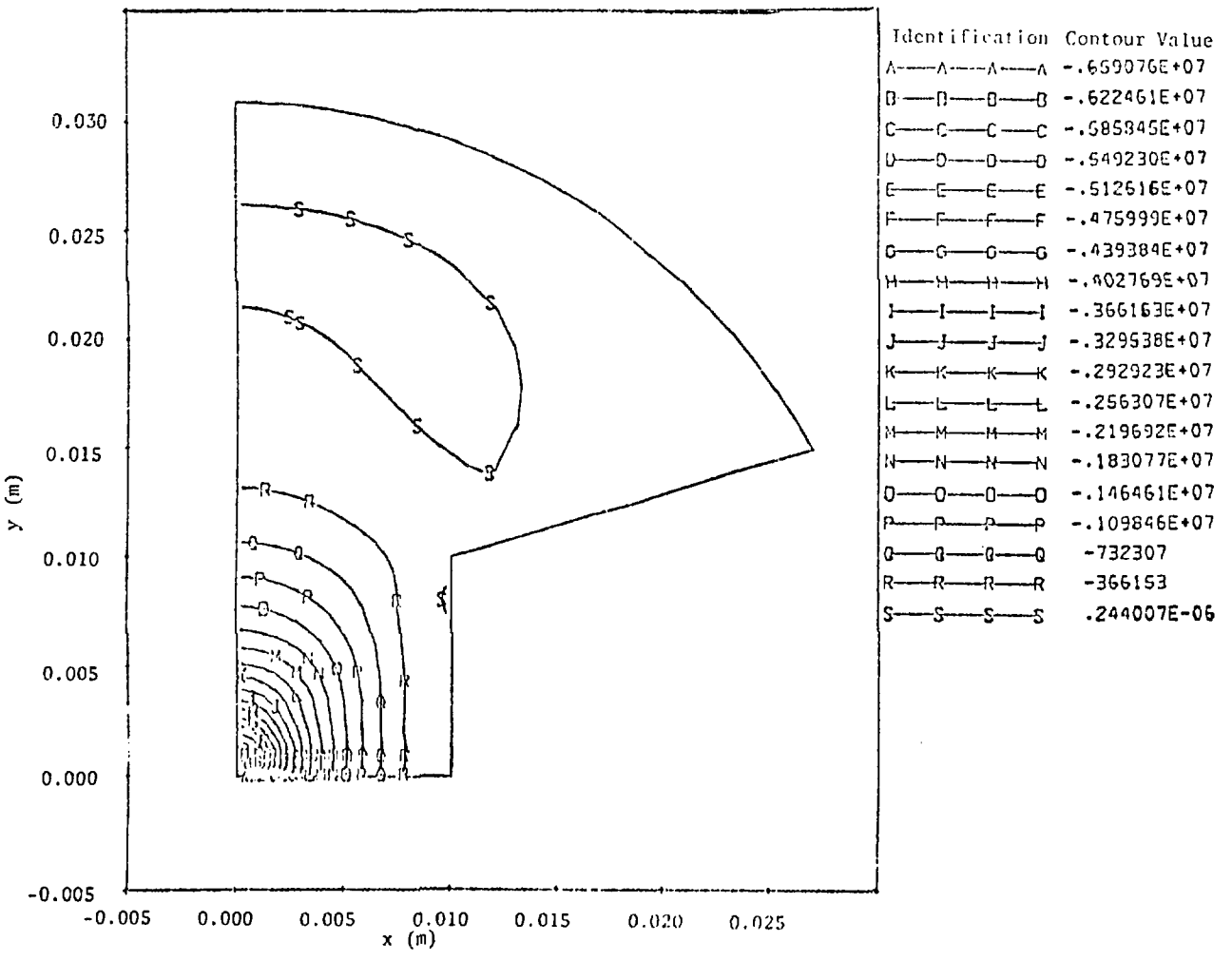

Fig. 12(c).
Minimum stress contours.

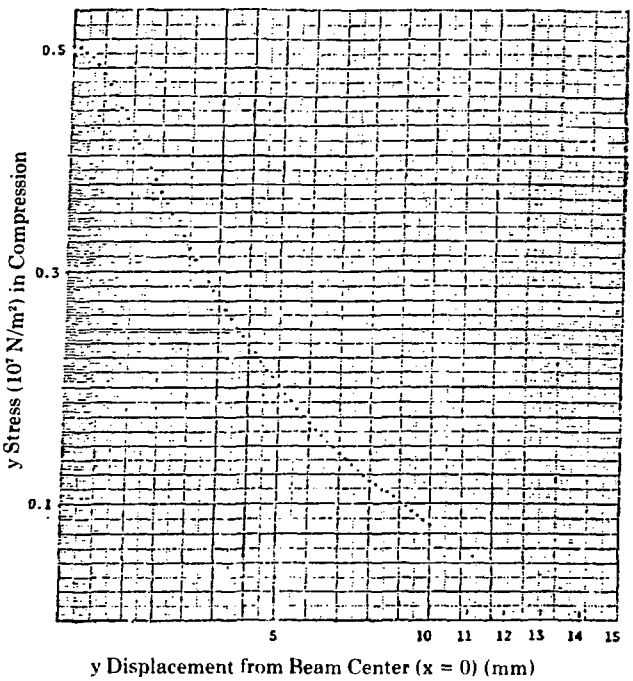

Fig. 13.
Plot of y-stress along x-axis.

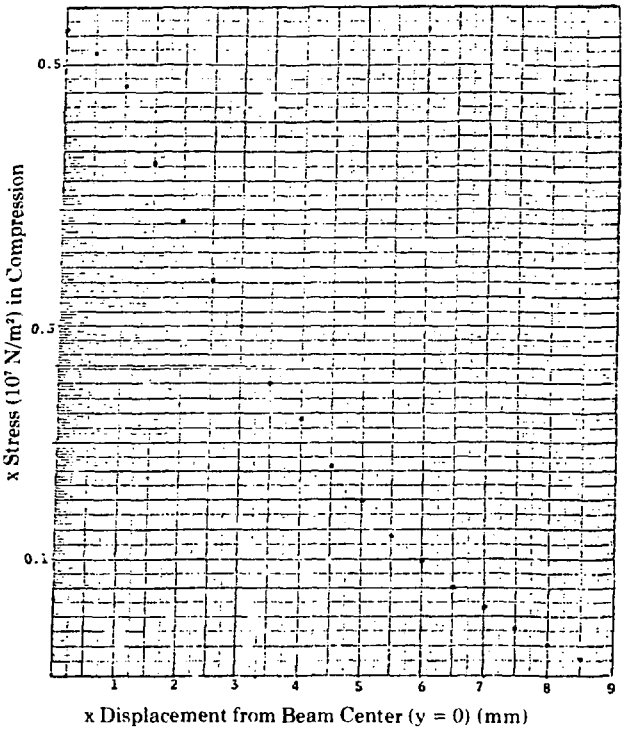

Fig. 14.
Plot of x-stress along x-axis.

APPENDIX

PYROLYTIC GRAPHITE PROPERTIES AS A FUNCTION OF TEMPERATURE

Four graphs (Figs. A-1 through A-4) present the 1) elastic modulus, 2) coefficient of thermal expansion, 3) thermal conductivity, and 4) specific heat of pyrolytic graphite. The "a" direction referred to lies in the crystalline plane of the material. The "c" direction is perpendicular to the planes. The black horizontal arrows indicate the temperature range considered.

Although the specific heat varies by a factor of 2 over this range, the specific heat determines only the calculational time for a steady-state solution — not the final temperature distribution. For convenience, the specific heat was set equal to a constant. The temperature distribution, on the other hand, is highly sensitive to the thermal conductivity. This varies by a factor of 5 over the region considered. The maximum value of the coefficient of the thermal expansion was used.[6]

REFERENCES

1. Lloyd O. Lindquist and Richard Main, "Graphite-to-Metal Bonding Techniques," Los Alamos Scientific Laboratory report LA-6928-MS (to be published).

2. R. J. Macek, private communication, 1976.

3. R. V. Browning, D. G. Miller, and C. A. Anderson, "TSAAS: Finite Element Thermal and Stress Analysis of Asymmetric Solids with Orthotropic Temperature-Dependent Material Properties," Los Alamos Scientific Laboratory report LA-5549-MS (May 1974).

4. Joseph F. Janni, "Calculations of Energy Loss, Range, Path Length, Straggling, Multiple Scattering, and the Probability of Elastic Nuclear Collisions for 0.1- to 1000-MeV Protons," Air Force Weapons Laboratory report AFWL-TR-65-150 (September 1966).

5. Arthur L. Edwards, "TRUMP: A Computer Program for Transient and Steady-State Temperature Distributions in Multi-Dimensional Systems," Lawrence Radiation Laboratory, UCRL-14754 Rev. 1 (May 1968).

6. Y. S. Touloukian *et al.*, ***The Thermo-Physical Properties of Matter Data Series*** (Plenum Publishing Corp., New York, 1970), Vols. 2 and 5.

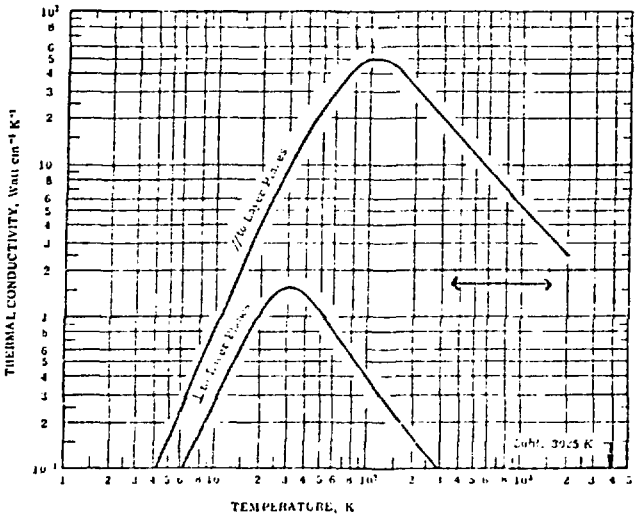

Fig. A-1.
Thermoconductivity of pyrolytic graphite vs temperature.

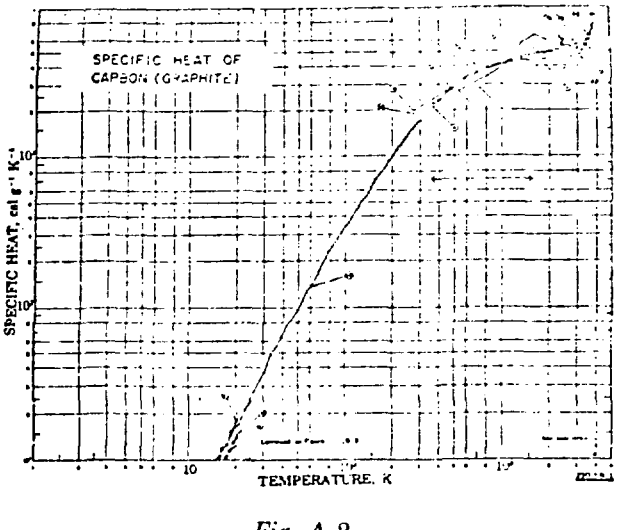

Fig. A-2.
Specific heat of carbon (graphite) vs temperature.

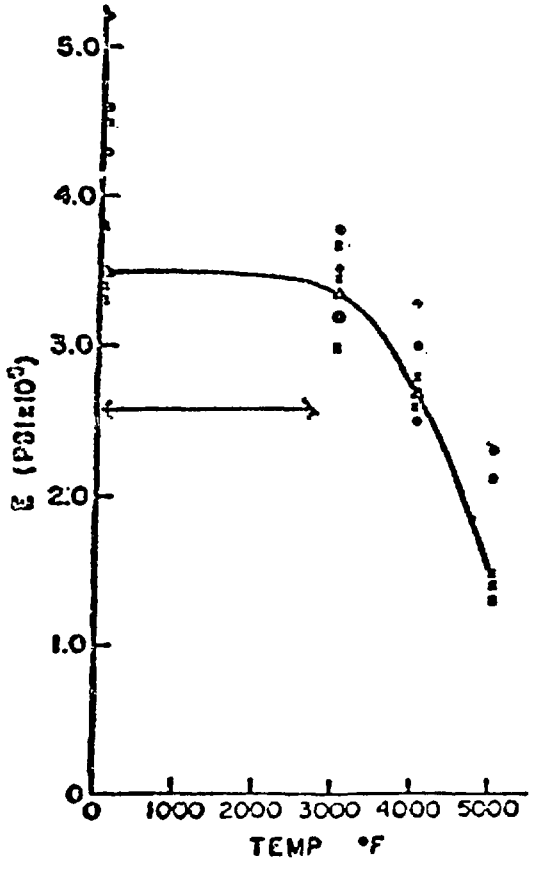

Fig. A-3.
Elastic modulus pyrolytic graphite "a" direction vs temperature.

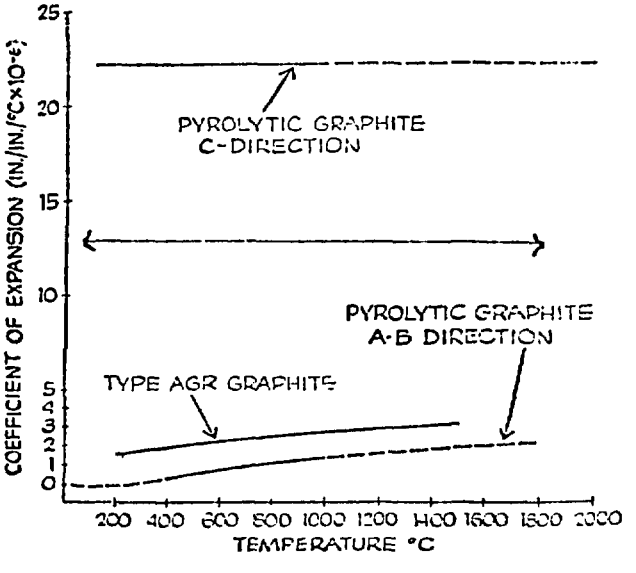

Fig. A-4.
Coefficient of thermal expansion of pyrolytic graphite vs temperature.

☆ U.S. GOVERNMENT PRINTING OFFICE: 1977—777-089/138